IAEA
International Atomic Energy Agency

20th IAEA Fusion Energy Conference
Vilamoura, Portugal, 1-6 November 2004

IAEA-CN-116/EX/P5-15

Observation of Current Profile Evolution Associated with Magnetic-Island Formation in Tearing-Mode Discharges on JT-60U

T. Oikawa, T. Suzuki, A. Isayama, N. Hayashi, T. Fujita, T. Tuda, G. Kurita, Y. Ishii and the JT-60 Team

**Naka Fusion Research Establishment,
Japan Atomic Energy Research Institute,
Naka, Ibaraki, 311-0193, Japan.**

Observation of Current Profile Evolution Associated with Magnetic-Island Formation in Tearing-Mode Discharges on JT-60U

T. Oikawa, T. Suzuki, A. Isayama, N. Hayashi, T. Fujita, T. Tuda, G. Kurita, Y. Ishii
and the JT-60 Team
Japan Atomic Energy Research Institute, Naka, Ibaraki, Japan

e-mail contact of main author: toikawa@naka.jaeri.go.jp

Abstract. Evolution of the current density profile associated with the magnetic island formation during a tearing mode was measured for the first time in JT-60U. With the island growth, the current density profile turned flat at the radial region of the island, followed by appearance of a hollow structure. As the island shrank, the deformed region became narrower, and it finally diminished after disappearance of the island. It was also observed that the local poloidal magnetic field from MSE fluctuated in correlation with a slow island rotation, confirming the existence of the perturbed current in the island O-point. The experimentally observed local hollow current density is reproduced in a time dependent simulation assuming reduction of the bootstrap current near the rational surface. Our observations are an experimental proof of reduction of the bootstrap current within the island O-point.

1 Introduction

Neoclassical tearing modes (NTMs) have been predicted to grow due to a helical deficit in the bootstrap current in the island O-point [1]. Several tokamaks have demonstrated suppressions of NTMs using electron cyclotron current drive (ECCD) with a highly localized driven current profile to replace the "missing" bootstrap current [2–4]. Recently, a substantial reduction in the ECCD power required for the NTM stabilization was demonstrated by an early ECCD injection in JT-60U [5]. A time-dependent NTM simulation indicates that an optimization of the ECCD profile can significantly reduce the EC power for stabilization [6]. The current density profile plays a key role in tearing modes. However, no observation of temporal dynamics of the current density profile has been reported for NTMs in high-temperature plasmas. In this paper, we report observations of the current density profile evolution associated with NTMs using a motional Stark effect (MSE) polarimetry [7, 8].

2 Measurement of Current Density Profile Evolution in an $m/n = 2/1$ Tearing Mode

A neutral beam (NB) heated H-mode discharge with an $m/n = 2/1$ tearing mode was investigated (Fig. 1). A tearing-mode-free discharge is also shown for comparison. Here, m and n are the poloidal and toroidal mode numbers, respectively. The vacuum toroidal magnetic field at the plasma center B_{t0} is 3.62 T, the plasma current I_{p} is 1 MA, and the safety factor at the flux surface with 95 % of the normalized poloidal flux q_{95} is 6.6. Neutral beam injection of 15 MW at a beam energy of 85 keV started at $t = 3.0$ s. Both discharges traced a similar temporal evolution of β_{N} (Fig. 1 (a-i)). In E36401, as shown in Fig. 1 (a-ii), the $n = 1$ magnetic perturbation appeared when the normalized beta β_{N} reached ~ 1 at $t \sim 3.3$ s. On the other hand, E36397 did not suffer any tearing mode in spite of reaching β_{N} comparable to or even higher than that in E36401. The reason is that the $q = 2$ surface did not exist (shown later) because current penetration was delayed due to a lower electron density than in E36401. In the $m/n = 2/1$ tearing mode discharge E36401, an electron cyclotron emission (ECE) radiometer with a sampling time of 20 μs shows that the corresponding perturbation in the electron temperature $\tilde{T}_{\mathrm{e}}$ existed around the $q = 2$ surface. Time evolutions of the frequency and amplitude at the peak of the $\tilde{T}_{\mathrm{e}}$ spectrum for an ECE channel located near the outer edge of the magnetic

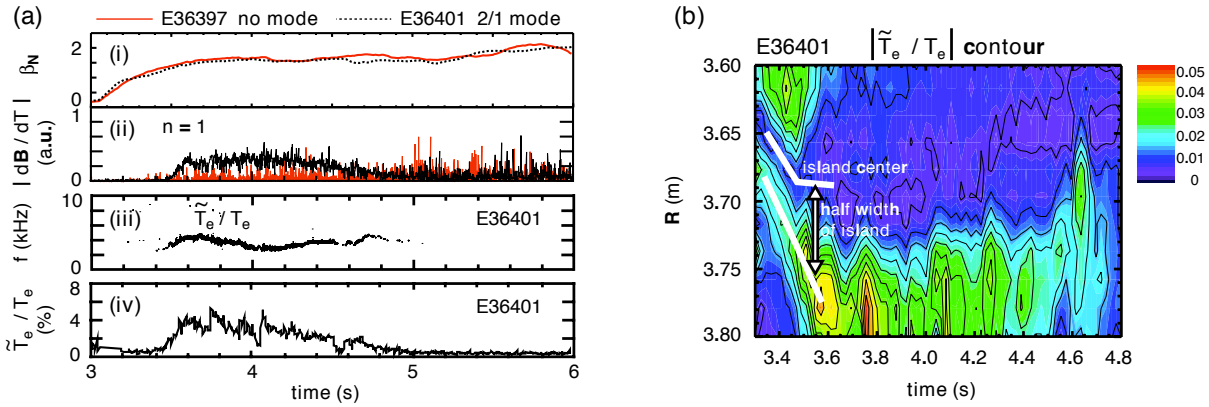

FIG. 1. **(a)** *Time histories of an $m/n = 2/1$ tearing mode discharge (E36401) and a quiescent discharge (E36397). (i) normalized beta $\beta_{\rm N}$, (ii) $n = 1$ magnetic perturbation at the wall (in time derivative), (iii) frequency spectrum of electron temperature perturbation $\tilde{T}_{\rm e}$ measured at $\rho \sim 0.4$ by ECE, and (iv) amplitude of $\tilde{T}_{\rm e}/T_{\rm e}$ at the frequency of the spectrum peak in (iii).*
(b) *Contour of amplitude of $\tilde{T}_{\rm e}/T_{\rm e}$ at the frequency of the spectrum peak. Evolutions of the O-point and outer edge of the island are indicated for the growth phase with the white thick lines.*

island ($\rho \sim 0.4$) are shown in Fig. 1 (a-iii) and (a-iv), respectively. The $m/n = 2/1$ tearing mode grew during $t = 3.3 - 3.6$ s and saturated. The magnitude of the tearing mode began to decrease at $t \sim 4.4$ s and disappeared at $t \sim 4.8$ s spontaneously. Figure 1 (b) shows the contour of amplitude of the fluctuating electron temperature $\tilde{T}_{\rm e}/T_{\rm e}$ at the island rotation frequency. The peaks of the $\tilde{T}_{\rm e}/T_{\rm e}$ profile indicated by light-colored areas indicate the inner and outer edges of the island. A half width of the island expanded from ~ 4 cm at $t = 3.35$ s to ~ 9 cm at $t = 3.6$ s. The inner peak deviated from the ECE viewing range at $t \sim 3.5$ s due to the island growth. The outward shift of the island center during $t = 3.3 - 3.6$ s resulted from the Shafranov shift associated with the increase in plasma beta. The island spontaneously began to shrink at $t \sim 4.4$ s and diminished at $t \sim 4.8$ s.

The current density profile is reconstructed with a magnetohydrodynamic (MHD) equilibrium code using data from an MSE diagnostic. With the use of a spline representation of the toroidal current density profile, our MHD equilibrium code is capable to give a reconstruction faithful to a small change in the MSE signals. Our MSE system has 15 channels with spatial resolution of $\Delta R = 6-10$ cm corresponding to $\Delta\rho = 0.05-0.15$ and a sampling time of 10 ms. Figure 2 shows the temporal evolutions of radial profiles of the current density $j(\rho)$ and safety factor $q(\rho)$ deduced by the equilibrium reconstruction with the MSE data for the $m/n = 2/1$ tearing mode discharge E36401. The current density is assumed to be zero at the surface in the equilibrium reconstructions. When the $m/n = 2/1$ tearing mode appeared at $t \sim 3.3$ s, $j(\rho)$ began to decrease and flatten around the $q = 2$ surface as shown at $t = 3.55$ s, at which the $q = 2$ surface located at $\rho = 0.27$ and the island extended in $\rho = 0.18 - 0.39$. The flat region around the $q = 2$ location became wider at $t = 3.7$ s. In the saturation phase ($t = 3.6 - 4.4$ s), a hollow structure appeared at the $q = 2$ location as shown at $t = 3.9$ s and 4.35 s. With the island shrinking from $t = 4.4$ s, j began to increase in the hollow region as observed at and after $t = 4.75$ s. This is considered to be recovery of the non-inductive current in the island O-point, as discussed later. Relaxation of a negative electric field generated by the increase in the non-inductive current caused the decrease in j inside the $q = 2$ surface ($t = 4.75$ s and 4.95 s). As a result, the $q = 2$ rational surface moved inward or diminished. Disappearance of the $m/n = 2/1$ tearing mode was considered to result from the inward shift of the $q = 2$ surface. The location or existence of the $q = 2$ surface is not clear at and after $t = 4.75$ s because there exists ambiguity in $j(\rho)$ inside the innermost MSE channel. After disappearance of the

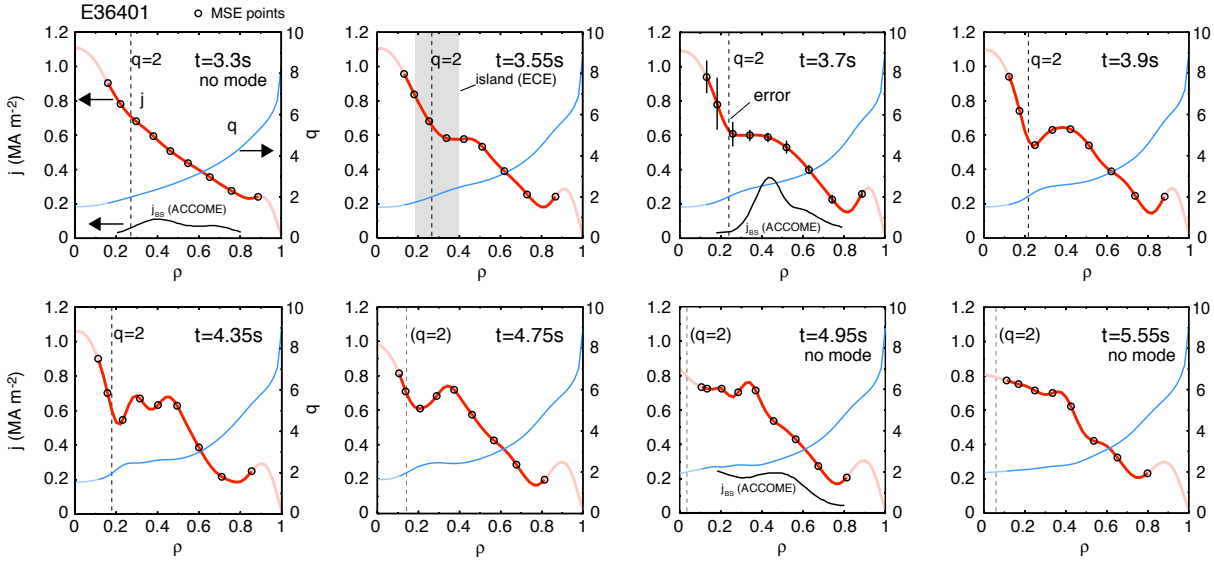

FIG. 2. Evolutions of the measured current density j and safety factor q profiles for E36401. The open circles indicate the MSE spatial points in the plasma. A typical error in $j(\rho)$ due to the statistical noise is shown at $t = 3.7$ s. Radial profiles of the calculated bootstrap current density $j_{\rm BS}$ are shown at $t = 3.3$ s, 3.7 s and 4.95 s. The dashed line at each time indicates the $q = 2$ location.

mode at $t \sim 4.8$ s, the hollow structure in $j(\rho)$ disappeared. In the analysis of the equilibrium reconstructions, four MSE channels covers the island region when the island fully evolved, as shown at $t = 3.55$ s of Fig. 2. Temporal change in j in the island region is larger than typical error due to the statistical noise as shown at $t = 3.7$ s. Thus, the spatial variation of the current density in the island region can be well resolved.

The evolution of the current density profile in the tearing-mode-free discharge E36397 is shown in Fig. 3 for comparison with the $m/n = 2/1$ tearing mode discharge above (E36401). The steady-state solution calculated by the ACCOME code is also shown, which is rather close to the measured profiles at $t = 5.2$ s. While it was observed that structures of neutral beam current drive (NBCD) and bootstrap current made some humps in the current density profile (Fig. 3), no deformation as observed in E36401 occurred. Thus, the deformation of the current density profile observed in E36401 is considered to result from the $m/n = 2/1$ tearing mode.

Expected causes for the observed deformation in $j(\rho)$ are flattening of the current density gradient owing to the classical tearing mode and reduction in the non-inductive current. In the present case, the non-inductive currents are the bootstrap current and co-NBCD. In Fig. 2, radial profiles of the bootstrap current density $j_{\rm BS}$ are calculated at $t = 3.3$ s, 3.7 s and 4.95 s, based on

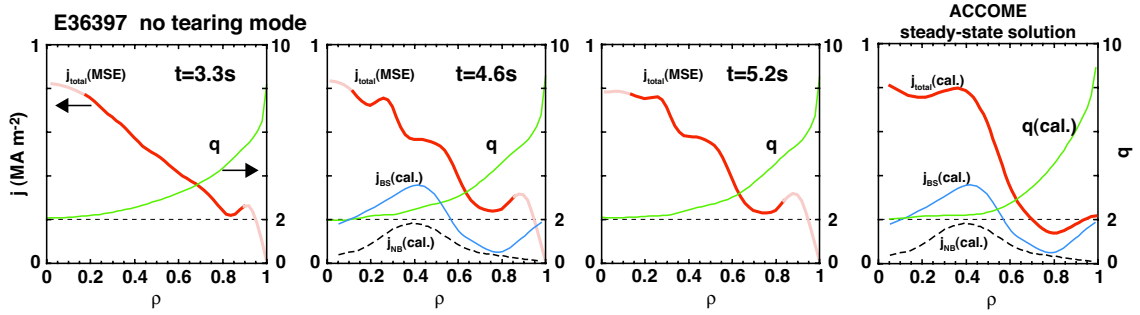

FIG. 3. Measured evolutions of $j(\rho)$ and $q(\rho)$ for the tearing-mode-free discharge E36397, and the steady-state solution by ACCOME using profiles at $t = 4.6$ s. Profiles of the calculated bootstrap current and NBCD are also shown at $t = 4.6$ s.

the measured profiles of the ion and electron temperature (T_i and T_e) and the electron density n_e. The measured profiles at $t = 3.7$ s are shown in Fig. 4. In the radial region of the island with small gradients of profiles, the bootstrap current is calculated nearly zero. Since time resolutions for the electron and ion temperature profiles are 25 ms and 50 ms, respectively, the measured temperatures are averages over a hundred of island rotations. Consequently, the flat regions in the temperature profiles are observed to be narrower than the island width identified by the ECE radiometer, and hence a finite bootstrap current density is calculated in the island region. Here, our calculation of the bootstrap current does not take into consideration an island structure. As a result, radial profiles with a flat region are treated to be uniform poloidally in the calculation, and the effect of finite orbits of the trapped particles are neglected. A recent result of a Monte Carlo simulation employing the δf method showed that a significant fraction of the ion bootstrap current survives inside the island O-point when the ion banana width is comparable to the island width, and that once the island grows, disappearance of the bootstrap current inside the island O-point is observed along with a small residual current near the island edge [9]. It was reported that in DIII-D NBCD at a beam energy of 75 keV was reduced as a result of fast ion transport when a large $m/n = 2/1$ island existed [10]. In JT-60U, on the other hand, we have observed that in the presence of a tearing mode fast ions injected at 360 keV suffered an anomalous transport but fast ions produced from neutral beam at a lower energy of 80-90 keV were not affected [11]. Thus, it is probable that inside the island O-point flattening of the current density gradient owing to the classical tearing mode and/or the loss of the bootstrap current cause the observed deformation in $j(\rho)$.

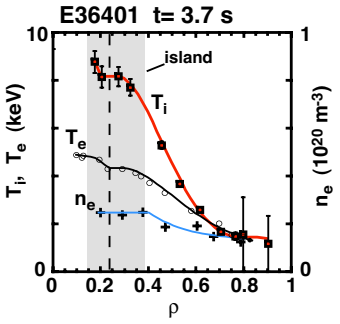

FIG. 4. Profiles of T_e, T_i and n_e for E36401 $t = 3.7$ s.

3 Role of Bootstrap Current in Temporal Dynamics of Current Density Profile

We discuss the observed evolution of the current density profile in the $m/n = 2/1$ mode plasma described above. Once the $m/n = 2/1$ tearing mode emerges and the island grows larger than some threshold (probably of the order of the poloidal ion Larmor radius), reduction of bootstrap current becomes in effect as a nonlinearly destabilizing term and it would overwhelm the stabilizing terms. The flattening around the island at $t = 3.7$ s is considered to result from the reduction in bootstrap current and the classical tearing mode process. We consider that with current diffusion in progress, reduction in bootstrap current in the island O-point appeared as a hollow structure around the $q = 2$ surface at $t = 3.9$ s. The hollow structure still remained at $t = 4.75$ s at which the tearing mode nearly disappeared and bootstrap current would mostly recover, and it disappeared $0.1 - 0.2$ s after that. We have done numerical simulations to elucidate such current profile evolution associated with bootstrap current reduction at the island (Fig. 5). Using a 1.5D transport code, temporal evolutions of current density profile have been calculated for two cases of pressure profile evolutions by taking into consideration NBCD and bootstrap current. In a first case, pressure profile is artificially flattened at the island, while pressure profile used in the second case is not flattened at the island. Here, in the first case we assume the flat pressure regions to be poloidally uniform, and hence it leads to overestimation of bootstrap reduction. However, it is expected that such simulations give us a view of temporal behavior of current density profile in NTM. In the simulation with the flattened pressure profile, the effect of bootstrap reduction at the island appears during the mode and the hollow structure still remains near the mode disappearance ($t = 4.75$ s), while there appears no deformation in the second simulation using the pressure profile without flat region. Thus, the observed current

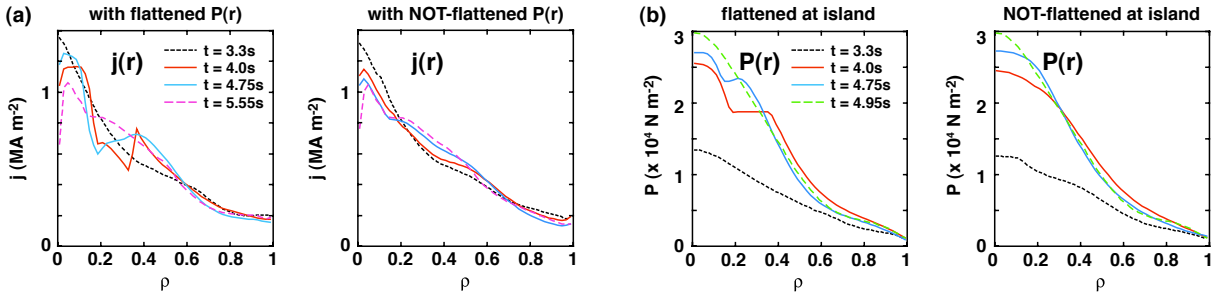

FIG. 5. Simulations of current profile evolution based on E36401. (a) current profiles at $t = 3.3$ s, 4.0 s, 4.75 s and 5.55 s for flattened pressure profile (left) and NOT-flattened pressure profile (right). (b) Pressure profile evolutions used in simulations, artificially flattened profile (left) and NOT-flattened profile (right). The flat region corresponds to the island structure measured by ECE at each time.

profile dynamics including formation of the hollow structure is qualitatively reproduced by introducing the bootstrap current reduction at the island.

Next, we discuss the role of bootstrap current reduction in the spontaneous inward shift of the $q = 2$ surface. The profile evolutions of current density j and loop voltage $V_{\rm loop}$ in E36401 are shown in Fig. 6 (a). Here, $V_{\rm loop}$ is calculated by $V_{\rm loop} = 2\pi R_0 \left(j_{\rm total}({\rm MSE}) - j_{\rm BS}({\rm cal.}) - j_{\rm NB}({\rm cal.})\right)/\sigma_{\rm neo.}$, where R_0 a typical major radius, $\sigma_{\rm neo.}$ the neoclassical conductivity, the bootstrap current $j_{\rm BS}$ and NBCD $j_{\rm NB}$ calculated by the ACCOME code. Different steady-state solutions are calculated by the ACCOME code using the measured temperatures and density profiles at $t = 3.9$ s (during mode) and $t = 4.95$ s (after mode) (Fig. 6 (b) and (c), respectively). It is considered that the spontaneous inward shift of the $q = 2$ surface was initiated due to an off-axis non-inductive current density profile. The NBCD profile has the peak around $\rho = 0.4 - 0.5$ during the whole discharge. The bootstrap current profile also has an off-axis peak during the tearing activity as shown in Fig. 6 (b), where reduction of the bootstrap current at the island makes a contribution. A large peak of the bootstrap current is due to a steep gradient in pressure profile just outside the island as shown in Fig. 4, which may be a result of the packing of flux surfaces due to the island O-point structure. Resultantly, the loop voltage $V_{\rm loop}$ profile during a initial transient phase has a hollow around $\rho \sim 0.45$ (Fig. 6 (a) $t = 3.7$ s). In the current diffusion process, $V_{\rm loop}$ is getting relaxed toward a spatially constant profile. Thus, it looks like that the inward shift of the $q = 2$ surface results from the decrease in $j_{\rm total}$ in $\rho < 0.4$ as a result of this current diffusion. The steady-state solution based on the profiles during mode ($t = 3.9$ s) (Fig 6 (b)) has $q(0) = 1.7$ and the $q = 2$ location at $\rho = 0.18$, while the measured $q(\rho)$ has $\rho_{q=2} = 0.21$. Although the current profile does not reach stationary at $t = 3.9$ s in the experiment, the steady-state solution is rather close to the measurement. If the magnetic island structure is maintained, i.e., the bootstrap current profile remains reduced at the island, the current profile is expected to evolve toward the calculated solution. As shown in Fig. 6 (c), on the other hand, the steady-state solution based on the profiles after the mode disappearance ($t = 4.95$ s) is clearly different from the measured profiles. The steady-state solution has a more peaked $j(\rho)$, lower $q(0) = 1.4$ and wider $\rho_{q=2} = 0.35$. This is because the current density profile is transient at $t = 4.95$ s due to recovery of the bootstrap current along with disappearance of the island. As shown in Fig 2, $j(\rho)$ became flat in $\rho < 0.3$ during $t = 4.75 - 4.95$ s, and $\rho_{q=2}$ rapidly moved further inward. It is considered that relaxation of a negative electric field generated by the bootstrap recovery at the rational surface causes the decrease in $j_{\rm total}$ inside the $q = 2$ surface. Summarizing the discussions, reduction and recovery of the bootstrap current at the rational surface explain the observed temporal dynamics such as the deformation in $j(\rho)$ and spontaneous inward shift of $\rho_{q=2}$.

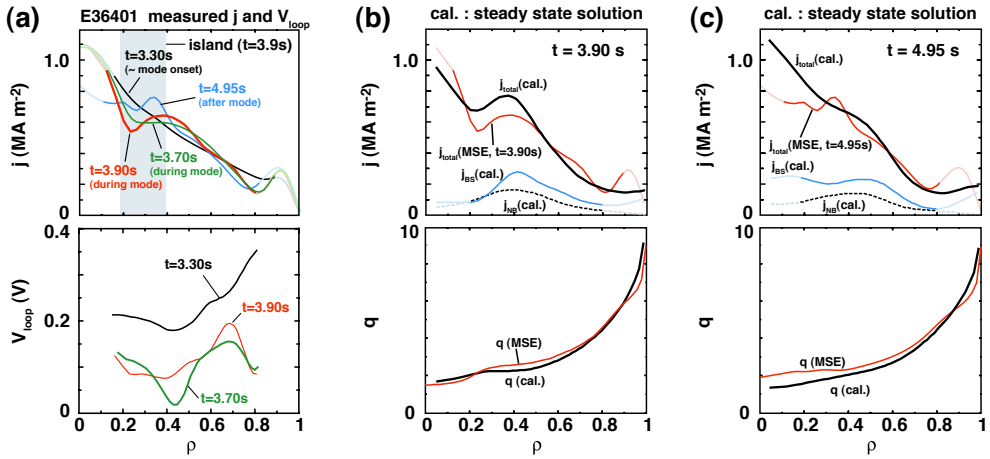

FIG. 6. Measurements and calculations for E36401. (a) Profiles of the measured current density $j_{\rm total}$ and loop voltage $V_{\rm loop}$. Comparisons of the measured $j(\rho)$ with the steady-state solutions by ACCOME at (b) $t = 3.9$ s (during the mode) and (c) $t = 4.95$ s (just after the mode disappearance).

4 Poloidal Asymmetry in Magnetic Perturbation Associated with Magnetic Island

We have to recall the following points on the experimental identification of the current density profile. A first point is on the treatment of an island structure in equilibrium reconstruction. As our equilibrium code does not treat equilibria with an island structure, a reconstructed equilibrium is the concentric flux surfaces with the single magnetic axis satisfying measurements within a convergence condition in a numerical calculation. The second point is the MSE measurement at a finite sampling time for a rotating island. The MSE signals are digitized at every 10 ms and averaged over several tens of milliseconds for reducing the statistical noise. At an effective time resolution, the measurement cannot resolve a variation correlated with the island rotation at $\sim 2-4$ kHz in the present case. Thus, we cannot distinguish whether the observed deformation in $j(\rho)$ in the $m/n = 2/1$ tearing mode discharge presented in section 2 is localized inside the island O-point or occurs uniformly in the poloidal direction for some reason. In order to clarify this point, we investigated a discharge with a stationary $m/n = 2/1$ tearing mode with intermittent mode lockings. The island expanded in $\rho \sim 0.5-0.7$. If deformation in $j(\rho)$ is localized inside the island O-point, the local poloidal magnetic field at the island would represent temporal variation correlated with the island rotation. In Fig. 7 (a), fluctuating electron temperatures at radii of the island, which were measured in the outboard equatorial plane, show that the island rotation was locked at $t = 7.27$ s and slowly rotated again. At the mode locking, an O-point of the $m/n = 2/1$ island structure existed in the outboard equatorial plane. Then, starting to rotate again, the X-point moved onto the outboard equatorial plane at $t \sim 7.37$ s. After some rotation, an X-point was situated in the outboard at $t = 7.59$ s. The local poloidal magnetic fields $B_{\rm p}$ were evaluated on the outboard equatorial plane directly from MSE. Figure 7 (b) shows time traces of $B_{\rm p}/B_T$ at and near the radial location of the island. We observed variations in $B_{\rm p}/B_T$ correlated with two 180 degree rotations at $t = 7.4-7.465$ s and $t = 7.535-7.59$ s (indicated by the dashed lines in Fig. 7 (b)), which are as slow as the MSE diagnostic can detect the corresponding changes. Time-lag between the ECE and MSE due to different spatial locations is negligibly small (several milliseconds) for the observed island rotations. At $\rho = 0.35$ and 0.44, the measured $B_{\rm p}/B_T$ increased for a rotation of X-point to O-point and decreased for a rotation of O-point to X-point. At and outside the radial location near the $q = 2$ surface, $B_{\rm p}/B_T$ behaved in the opposite manner. There observed little change at $\rho = 0.53$ (near the inner island edge). This observation has been validated with a classical tear-

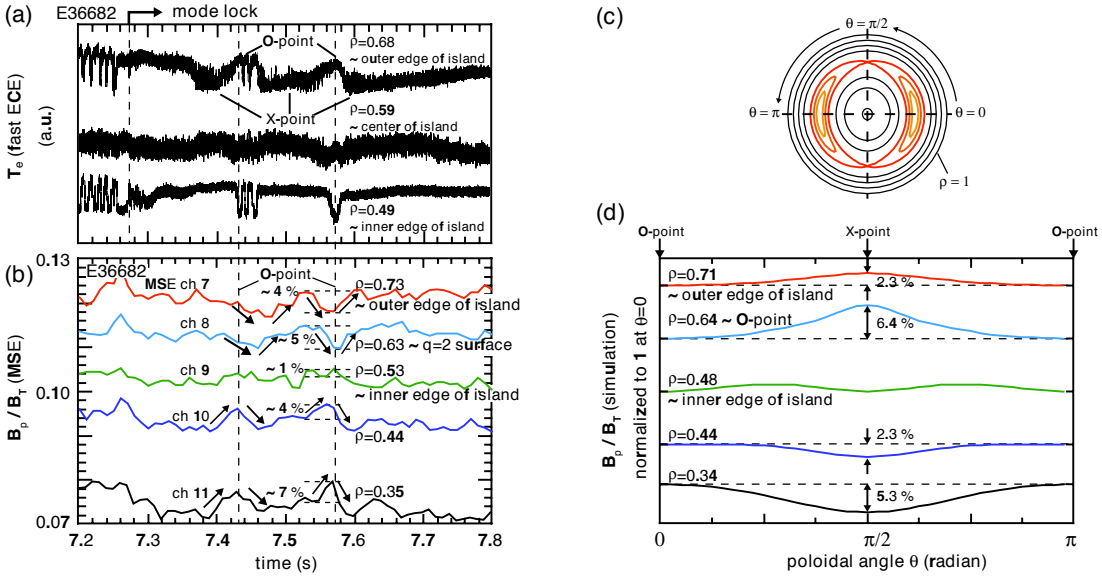

FIG. 7. Time evolutions of E36682 with a stationary $m/n = 2/1$ tearing mode with the saturated island at $\rho \sim 0.5 - 0.7$. (a) The fluctuating T_e at the inner and outer edges of the island and the O-point (measured by the ECE radiometer). (b) B_p/B_T at MSE measurement points around the island. A classical tearing mode simulation reproduces the $m = 2/n = 1$ island at $\rho = 0.48 - 0.71$. (c) Contour of the helical poloidal flux function. (d) Poloidal distributions of B_p/B_T at the radii corresponding to the MSE points in (b). The values are normalized at $\theta = 0$.

ing mode simulation using a nonlinear resistive MHD code. The $m/n = 2/1$ island structure at $\rho = 0.48 - 0.71$ is reproduced as shown in Fig. 7 (c), where an O-point stays at the $\theta = 0$ plane. Figure 7 (d) shows a calculated poloidal distributions of B_p/B_T at the same radii in Fig. 7 (b). The variation in B_p/B_T between O- and X-points at each radial location agrees reasonably with the observation. Thus, we clarified that the observed deformation in $j(\rho)$ was localized inside the island O-point.

5 Direct Evaluation of Current Profile Evolution Associated with a Narrow Magnetic Island Formation and its Suppression using ECCD

We present a direct evaluation of $j(\rho)$ from MSE without equilibrium reconstruction, which is useful when variation in $j(\rho)$ is localized in a narrow region comparable to the spatial resolution of MSE. Figure 8 (a) shows an $m/n = 3/2$ NTM that appeared at $t = 5.3$ s in a plasma with $\rho(q = 3/2) \sim 0.5$. The m/n = 3/2 NTM was completely stabilized at $t = 8.7$ s by ECCD. After the switch-off of the EC injection, the m/n = 3/2 NTM was destabilized again. Figure 8 (b) shows the evolution of the current density change δj from $j(\rho)$ at $t = 5.4$ s, where δj is evaluated directly from the MSE sig-

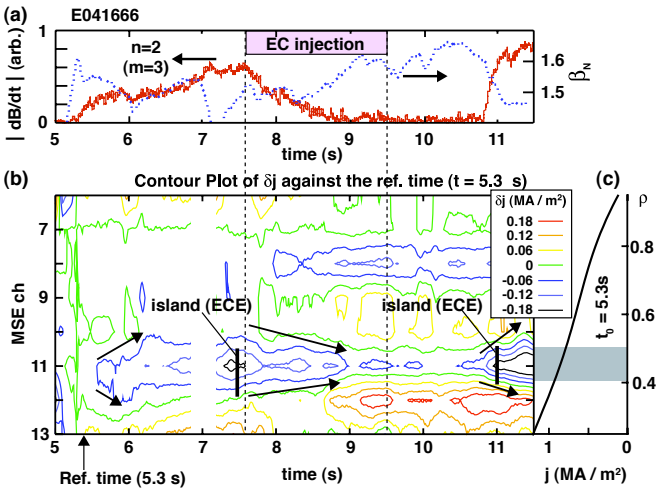

FIG. 8. Evolution of an $m/n = 3/2$ NTM discharge. (a) $n = 2$ magnetic fluctuation and β_N, and (b) temporal variation of the current density profile from the one at $t = 5.4$ s shown in (c).

nals based upon the reference equilibrium at $t = 5.4$ s by using an analysis technique in ref. [8], because it is rather difficult to reproduce equilibrium corresponding to a small change in the narrow region of the $m/n = 3/2$ island. At $t = 5.7$ s, a negative δj region appeared at $\rho \sim 0.4$ (MSE ch 11) and expanded. The location and saturated width of the negative δj region agreed with the island structure identified in the $\tilde{T}_e$ profile measured by ECE. As the $m/n = 3/2$ NTM was suppressed by ECCD, the negative region became narrower and finally disappeared at $t = 8.9$ s when the NTM was completely stabilized. After the turn-off of the EC injection at $t = 9.5$ s, the $m/n = 3/2$ NTM reappeared at $t = 10.8$ s and a region of negative δj expanded at the island location again.

6 Conclusions

We have shown the dynamics of the current profile associated with the magnetic island formation in JT-60U tearing mode plasmas using MSE. We observed the transition of the current profile to the flat and hollow structure at the island. This deformed structure gradually diminished with the shrink and disappearance of the island. We also observed that the local poloidal magnetic field from MSE fluctuated in correlation with the slow island rotation, confirming the existence of the perturbed current in the island O-point. The experimentally observed local hollow current density is reproduced in the time dependent simulation assuming reduction of the bootstrap current near the rational surface. Comparisons of the measurements with the calculated steady-state solution also explain the temporal behaviors of the current density and safety factor profiles with reduction and recovery of the bootstrap current. Our observations are an experimental proof of reduction of the bootstrap current within the island O-point.

In the discharge with the narrow $m/n = 3/2$ magnetic island, using the direct evaluation of the current density profile from MSE without equilibrium reconstruction, we also found reduction of the current density at the narrow island region and its recovery due to the local ECCD.

Acknowledgment The authors would like to thank T. Ozeki for many helpful discussions.

References

[1] CARRERA, R., HAZELTINE, R.D., and KOTSCHENREUTHER, M., Phys. Fluids **29** (1986) 899.

[2] ZOHM, H., *et al.*, Nucl. Fusion **39** (1999) 577.

[3] ISAYAMA, A., *et al.*, Plasma Phys. Control. Fusion **42** (2002) L37.

[4] PETTY, C., *et al.*, Nucl. Fusion **44** (2004) 243.

[5] NAGASAKI, K., *et al.*, this conference, EX/7-4.

[6] HAYASHI, N., *et al.*, Nucl. Fusion **44** (2004) 477.

[7] OIKAWA, T., *et al.*, submitted to Phys. Rev. Lett.

[8] SUZUKI, T., *et al.*, J. Plasma Fusion Res. **80**, 362 (2004).

[9] POLI, E., *et al.*, Phys. Rev. Lett. **88** (2002) 075001-1.

[10] FOREST, C.B., *et al.*, Phys. Rev. Lett. **79** (1997) 427.

[11] OIKAWA, T., *et al.*, Nucl. Fusion **41** (2001) 1575.